Hindawi
Advances in Civil Engineering
Volume 2022, Article ID 5018645, 10 pages
https://doi.org/10.1155/2022/5018645

Research Article

A Mesoscale Approach for Concrete Block Masonry

Xu Yang,[1,2] Mingming Jia,[2] Bin Chi,[3] Mingzhi Wang ,[2] and Jianfeng Zheng[4]

[1]*Institute of Engineering Mechanics, China Earthquake Administration, Key Laboratory of Earthquake Engineering and Engineering Vibration of China Earthquake Administration, Harbin 150001, China*
[2]*School of Civil Engineering, Harbin Institute of Technology, Harbin 150090, China*
[3]*Suzhou University of Science and Technology, Suzhou, China*
[4]*Transportation and Construction Bureau of Pingtan Comprehensive Pilot Zone, Fujian, China*

Correspondence should be addressed to Mingzhi Wang; mwang@hit.edu.cn

Received 14 December 2021; Revised 17 March 2022; Accepted 23 March 2022; Published 21 July 2022

Academic Editor: Cong Zhang

A comprehensive understanding of the concrete block masonry's mesostructure on its macroscopic mechanical behavior is meaningful for modern masonry. The mesoscale numerical method provides an extremely powerful analyzing tool for this problem. However, it is still difficult to analyze the mesomodel efficiently due to a large number of operating processes caused by the components' nonlinear mechanical properties. An efficient finite-element-method-based mesoscale approach for concrete block masonry was introduced in this paper. The benchmark test results obtained show that this approach is able to simulate the concrete block masonry and analyze its failure. According to the simulation studies, a positive effect of mortar and concrete block strength on masonry compressive strength was obtained. Besides, an obvious nonlinear relationship between the masonry compressive strength and the mortar was also observed.

1. Introduction

Concrete block masonry is widely applied in various modern buildings. Its mechanical behavior has received increased attention in recent years.

Currently, there is little doubt that the behavior of concrete block masonry is strongly influenced by the mechanical properties of its components at the mesolevel [1]. Therefore, analyzing this structure at the mesoscale should be extremely powerful for understanding and predicting the observed macroscopic mechanical behavior. Especially, the concrete block masonry is usually treated as quasibrittle material [2]; it is difficult to devise the experimentations. The numerical method is not limited by experimental equipment or sites, and thus, precise results can be conveniently obtained. Researchers only need to establish a reasonable mesomodel of the concrete block masonry, considering the geometrical parameters and material properties of each component. The numerical mesomodel can then be utilized to ascertain the influence of components on the mechanical behavior of concrete block masonry or to simulate loading conditions that are difficult to achieve in the laboratory [3–9].

Concrete block masonry is generally considered a three-phase composite on the mesoscale, consisting of concrete block, mortar, and the interfacial transition zone (ITZ) between these two [1, 10, 11]. The ITZ simulation methods of concrete block masonry under compression could then be divided into three categories according to the assumption: tie mode, friction mode, and cohesion mode [1, 12].

First, in the framework of the tie mode, the concrete masonry unit and mortar were assumed to be well bonded and there would be none of the deformation slips during the process of concrete block masonry prism under compression [13–16]. Barbosa et al. proposed a combined experimental program and numerical model to study the performance of ungrouted concrete masonry block prisms [17]. They demonstrated the predictions of peak load and failure mode of concrete masonry prism under compression are in good agreement with experimental results [18].

Since this type of simulation method aims to establish a simplified model which could obtain the maximum compressive strength of concrete masonry prism quickly, the deformation of concrete masonry prism could not be precisely simulated.

Second, the friction mode proposes an ITZ model by using the discrete cracking model with the friction assumption [19–21]. As introduced in previous studies, the concrete masonry and mortar are modeled separately, while the mechanical behavior between them is employed using the "surface-to-surface" interaction property [22]. The interaction property involved two directional parameters: normal and tangential mechanical behavior. The normal behavior keeps the unit and mortar stay in contact and would not sink into each other when under a compression load. Meanwhile, the separation is allowed between the concrete block and mortar when the ITZ bears a tension load. The coulomb frictional theory was adopted to describe the tangential behavior. This numerical method considered the longitudinal relative displacement between block and mortar when the displacement force exceeds the critical shear stress. The above research studies demonstrate the numerical model could successfully predict the compressive strength, global stiffness, and stress-strain curves of concrete masonry prism under compression. Nevertheless, the neglect of the influence of interfacial adhesion in this simulation method caused its downside in analyzing the concrete masonry prism under shear loading.

Recently, some researchers introduced the cohesive method into the contact property between concrete masonry unit and mortar, which is named "cohesion mode" [23–25]. Several researchers expanded the units up to half of the mortar thickness in horizontal and vertical directions as continuum elements, while the interface between the continuum elements was used adhesives-cohesive behavior [26, 27]. The adhesives-cohesive behavior can provide the traction-separation response and fracture modes of the interface, and the relative parameters are determined by the material strength of the mortar. A good agreement could be found between the numerical and experimental results of concrete masonry prism under compression, shear, and diagonal tension. Nevertheless, many parameters in this method are needed to be treated and assumed due to lacking efficient information and the disadvantages of relatively complex modeling, larger calculation time also limits its application scope.

In conclusion, because of the large number of the operating process caused by the components' nonlinear mechanical properties, it is still difficult to analyze the mesomodel efficiently. In the present study, an efficient finite-element-method-based mesoscale approach for concrete block masonry was introduced. The benchmark test results demonstrated that this approach is suitable for simulating the concrete block masonry and analyzing its failure. Furthermore, based on the numerical case study, the effect of the components on the concrete block's macroscopic mechanical behavior was studied and discussed.

2. Method

2.1. Mesoscale Geometrical Model of Concrete Block Masonry. In general, as represented in Figure 1, the concrete block masonry could be considered as a three-phase composite on the mesoscale, consisting of concrete block, mortar, and the interface transition zone between them [1, 11].

In particular, concrete block, as a concrete product, could usually be treated as elastic. The constitutive behavior of the concrete block was formulated based on linear elastic damage mechanics in this paper, using the maximum tensile strain criterion as the threshold.

The mortar thickness is commonly between 8 and 12 mm. In the numerical model proposed in this study, the mortar was formulated based on linear elastic damage mechanics with the maximum tensile strain criterion as the threshold, as well. As the dimension of mortar was much smaller than that of concrete block, it should be noticed that mesh size should be set carefully.

ITZ locates between the concrete block and the mortar. The ITZ's mechanical properties influence the failure pattern and load-carrying capacity of the masonry. It should be noticed that the ITZ thickness is difficult to be measured [10]. Thus, the ITZ is defined as a thin layer with a finite thickness (larger than zero) in several studies [28], or a zero-thickness boundary layer in other studies [29, 30]. Therefore, the thickness of ITZ was considered as 1 mm to simplify the model, i.e., 10% of the mortar thickness, in this study. The constitutive law for the ITZ employed in this approach conforms to the failure criterion proposed in [31]. Denoting the shear and tensile strengths of ITZ as f_s^{ITZ} and f_t^{ITZ}, respectively, the failure surface $S_{\mathrm{failure}}^{ITZ}$ is defined as the following three-parameter hyperbola:

$$S_{\mathrm{failure}}^{\mathrm{ITZ}} = \tau^2 - \left(\sigma - f_s^{\mathrm{ITZ}} \tan\varphi\right)^2 + \left(f_t^{\mathrm{ITZ}} - f_s^{\mathrm{ITZ}} \tan\varphi\right)^2, \quad (1)$$

where τ is the shear stress, σ is the normal stress, and φ is the asymptotic friction angle, which is defined as 27° according to [31].

2.2. Numerical Method. The geometrical model generated based on the method introduced in Section 2.1 could be solved by the finite element method considering failure process, which was named as kill-FEM in this study. The basic iterative algorithm of kill-FEM represented in Figure 2 for finite element analysis could be described as follows.

2.2.1. Based on the Geometrical Dimension, Generate an Initial Finite Element Model. First, as shown in Figure 3, the geometrical model generated could be divided into standard four-noded tetrahedral or eight-noded hexahedral finite elements. This meshing step was carried out on ABAQUS (version 2020), which provides an adaptive mesh module with general applicability. After reading and converting the mesh results to the format could be processed in python by implementing meshio tool [32], the global nodal forces $\{F^{(0)}\}$ and the global nodal displacements $\{d^{(0)}\}$ in this initial model could be related through the global stiffness matrix $[K^{(0)}]$,

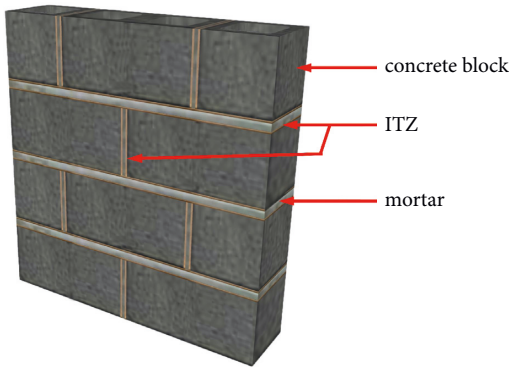

Figure 1: Schematic diagram of concrete block masonry's mesomodel.

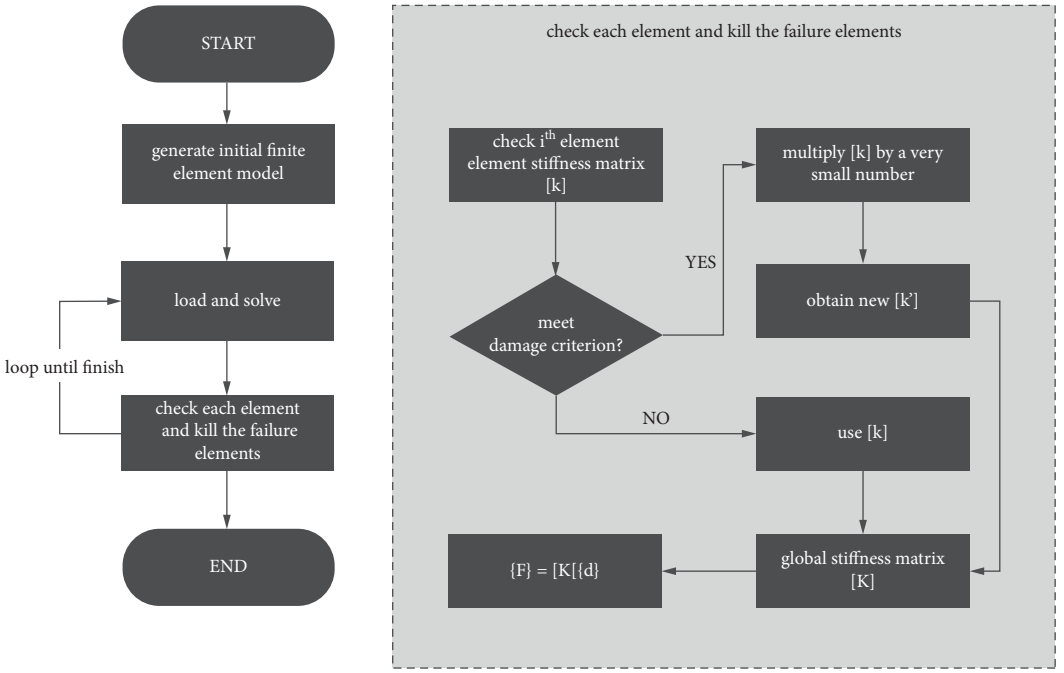

Figure 2: Schematic diagram of solving the numerical model based on kill-FEM.

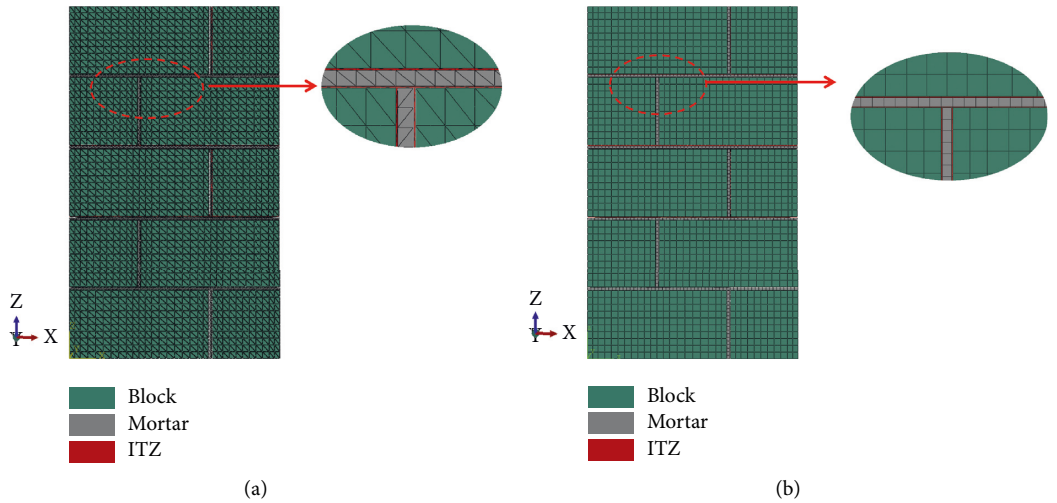

Figure 3: Finite element mesh of the concrete block masonry. (a) Four-noded tetrahedral element. (b) Eight-noded hexahedral element.

which could be given by the classic equation $\{F^{(0)}\} = [K^{(0)}]\{d^{(0)}\}$. Denoting the element stiffness matrix as $[k]$ of an element, the global stiffness matrix could be obtained by assembling element stiffness matrices simply. According to the definition of the tetrahedral or hexahedral element, $[k]$ would be influenced by the shape of the element, elastic modulus, Poisson's ratio, and the constitutive model.

2.2.2. Analyze This Finite Element Model, Find the Failure Elements, and Then Kill These Elements. After solving the initial model, all stress and strain values of all the elements could be obtained. Each element would be then validated based on the damage criterion mentioned above. Specifically, the concrete block and the mortar elements would be checked whether their principal strain meets the maximum tensile strain criterion; the ITZ elements would be checked whether they meet the criterion given by equation (1). Once the damage criterion was met, the element would be "killed" by multiplying the element stiffness $[k]$ by a very small number α, for example, $\alpha = 10^{-14}$ was employed in this study. Therefore, the element stiffness of the killed element $[k'] = \alpha[k]$ could be obtained. As well, the global stiffness matrix of the first step $[K^{(1)}]$ could be obtained by assembling $[k']$ of all elements. Obviously, these killed elements could remain in the model but contribute a near-zero stiffness to the whole model.

2.2.3. Analyze the Finite Element Model with Killed Elements. Then, input the global nodal forces $\{F^{(1)}\}$ and global nodal displacements $\{d^{(1)}\}$ in the first step model and relate them through $[K^{(1)}]$. The matrix equation of this model $\{F^{(1)}\} = [K^{(1)}]\{d^{(1)}\}$ could be obtained. The model in the first step could be solved. We could repeat steps (b) and (c) until the finish.

This method can be used for efficient simulation of quasibrittle materials subjected to forces.

3. Numerical Case Study

3.1. Materials. The masonry prism for simulating consisted of concrete block, mortar, and the ITZ between them.

The dimension of concrete block was represented in Figure 4. Actually, the diagonal dimension of the hole should be controlled by a small round corner, which had been simplified in this study.

The mechanical properties of concrete were applied for simulating the block, i.e., the elastic modulus E_b, Poisson's ratio μ_b, and maximum tensile strain $\epsilon_{\max,b}$, which would be measured in the standard concrete material testing. It should be noticed that several researchers employed the mechanical properties measured by concrete block directly for simulating the block, we could barely agree on which. A concrete block, for example, which is represented in Figure 4, could already be considered as a structure or a production made by concrete and the mechanical properties of a block must not be equal to those of concrete obviously. Since the block would be divided into a set of elements by employing mesh technology naturally, each element then contributed to the whole masonry prism's mechanical behaviors. This element type was the concrete, which should be assigned the properties of the concrete, i.e., the base material of the block. Employing wrong mechanical parameters of materials would cause implausible simulation results.

Additionally, the following mechanical properties were applied for simulating the block, i.e., the elastic modulus E_m, Poisson's ratio μ_m, and maximum tensile strain $\epsilon_{\max,m}$, which would be measured in the standard construction mortar material testing.

Since the elastic modulus E_{ITZ} and Poisson's ratio μ_{ITZ} were difficult to be measured in the experiments, the value of E_{ITZ} was approximately set as 0.8 times E_m according to the proposal in previous studies and μ_{ITZ} was set as 0.15 [33].

3.2. Concrete Block Masonry under Compression. In this section, a group of benchmark tests was simulated for validation of the numerical method first. As shown in Figure 5, the dimensions of the masonry wallets tested were 590 mm length, 990 mm height, and 190 mm thickness. These corresponded to five courses of concrete block vertically, on and a half blocks horizontally, and on block transversely. The mechanical properties of concrete block and mortar, as well as the shear and tension strength of ITZ, were measured in our previous study. More details about the experimentation could be found in [34]. Besides, the elastic modulus and Poisson's ratio of ITZ were obtained based on the mortar parameters, according to the manners introduced in Section 3.1. All material parameters mentioned above of these three components are represented in Table 1, based on which the benchmark models for validation were simulated.

Then, the effect of concrete block and mortar mechanical properties on the masonry was discussed based on different components' material parameters, i.e., the concrete block and the mortar material properties are assigned as in Tables 2 and 3, respectively. The varied combinations were simulated.

4. Results and Discussions

4.1. Benchmark Test Results. Before all, the numerical modeling method should be validated by comparing the simulation results with the experimental ones. The concrete block masonry's compressive strength was usually considered as one of the most important indexes in engineering and research, based on which the simulation would be discussed.

Denoting the concrete block masonry's compressive strength measured in the tests as the x-coordinate and the strength obtained from simulation as the y-coordinate, respectively, the comparison point could then be plotted in a scatter plot as shown in Figure 6.

Additionally, a straight reference line of $y = x$ was added in the scatter. This line could indicate the location that simulation results are equal to the testing results, which made the plot more intuitive. The points plotted in Figure 6 could be observed that located beside the reference line, which demonstrated a good agreement with the testing

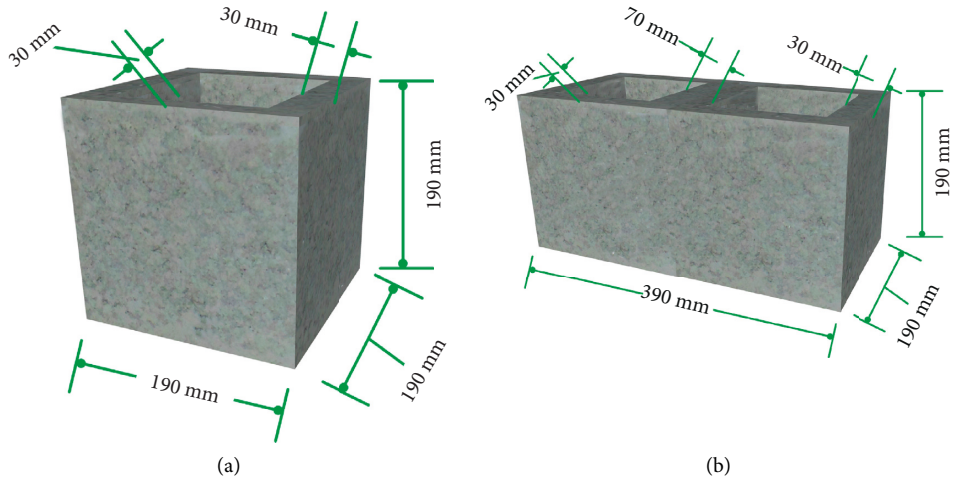

Figure 4: Dimensions of concrete blocks (all dimensions are in mm). (a) Concrete type A. (b) Concrete type B.

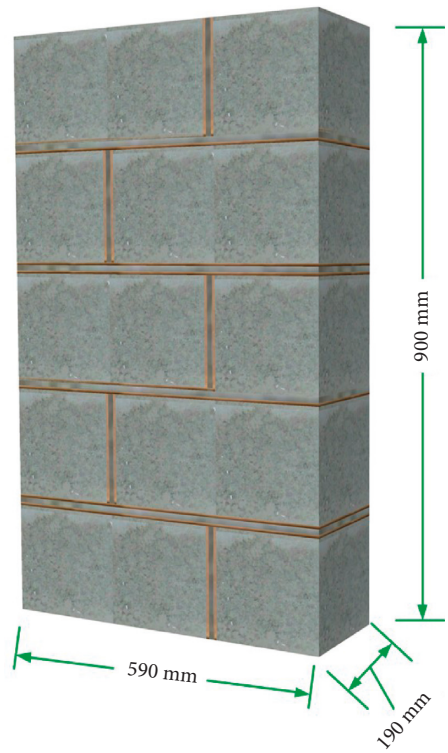

Figure 5: Dimensions of masonry wallets (all dimensions are in mm).

Table 1: Various components' material parameters used for modeling.

No.	E_b (MPa)	μ_b	ϵ_b (10^{-6})	E_m (MPa)	μ_m	ϵ_m (10^{-6})	E_{ITZ} (MPa)	μ_{ITZ}	f_s^{ITZ} (MPa)	f_t^{ITZ} (MPa)
1	12006	0.20	117	5940	0.15	106	4752	0.15	2.72	0.29
2	11609	0.20	112	5676	0.15	103	4541	0.15	2.60	0.29
3	12437	0.19	116	6161	0.15	101	4929	0.15	2.73	0.30
4	18115	0.20	142	5940	0.15	106	4752	0.15	2.62	0.29
5	17254	0.20	135	6064	0.15	109	4851	0.15	2.66	0.28
6	18918	0.20	139	6042	0.15	101	4834	0.15	2.63	0.29
7	18115	0.20	142	15234	0.15	102	12187	0.15	2.79	0.30

Table 1: Continued.

No.	E_b (MPa)	μ_b	ϵ_b (10^{-6})	E_m (MPa)	μ_m	ϵ_m (10^{-6})	E_{ITZ} (MPa)	μ_{ITZ}	f_s^{ITZ} (MPa)	f_t^{ITZ} (MPa)
8	17403	0.19	142	15452	0.15	104	12361	0.15	2.85	0.30
9	18907	0.19	147	14606	0.14	107	11685	0.15	2.85	0.29
10	29435	0.20	106	15234	0.15	102	12187	0.15	2.62	0.29
11	29436	0.19	108	15086	0.15	106	12069	0.15	2.61	0.30
12	29138	0.20	106	14587	0.14	102	11669	0.15	2.61	0.28

Table 2: Concrete block's material parameters.

Type	E_b (MPa)	μ_b	ϵ_b (10^{-6})
MU7.5	7500	0.2	100
MU10	10000	0.2	100
MU15	15000	0.2	100
MU20	20000	0.2	100
MU25	25000	0.2	100

Table 3: Mortar and ITZ's material parameters.

Type	E_m (MPa)	μ_m	ϵ_m (10^{-6})	E_{ITZ} (MPa)	μ_{ITZ}	f_s^{ITZ} (MPa)	f_t^{ITZ} (MPa)
Mb5	7624	0.15	66	6099	0.2	2.72	0.29
Mb7.5	9843	0.15	76	7875	0.2	2.77	0.28
Mb10	11799	0.15	85	9439	0.2	2.74	0.28
Mb15	15233	0.15	98	12187	0.2	2.79	0.29
Mb20	182601	0.15	110	14608	0.2	2.73	0.30

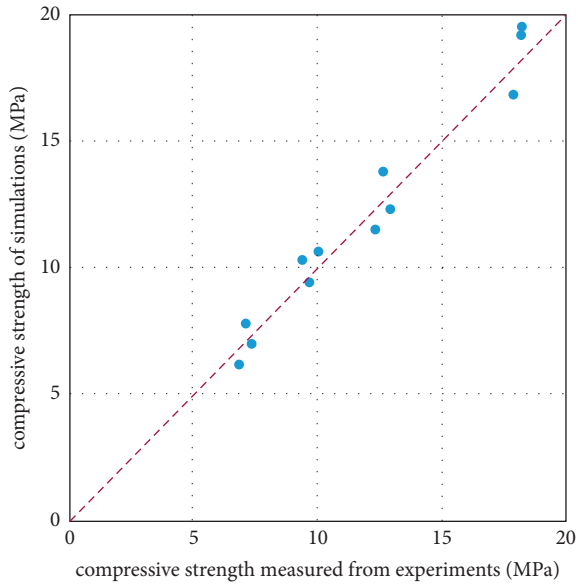

Figure 6: Comparison of simulated and experimental compressive strengths.

results. According to this numerical benchmark test results which were consistent with the fact, the numerical method proposed could be basically considered practical.

4.2. Failure Pattern. In addition to the compressive strength, the failure pattern could also represent the mechanical characteristics of masonry. The simulation failure pattern would therefore be compared with the experimental results and discussed in this section.

By applying the modeling method introduced, the cloud charts of principle tensile strain, displacement magnitude, and 1^{st} principle stress could be drawn, which are represented in Figure 7.

As a quasibrittle material, the concrete block masonry could be recognized as that meeting the maximum tensile

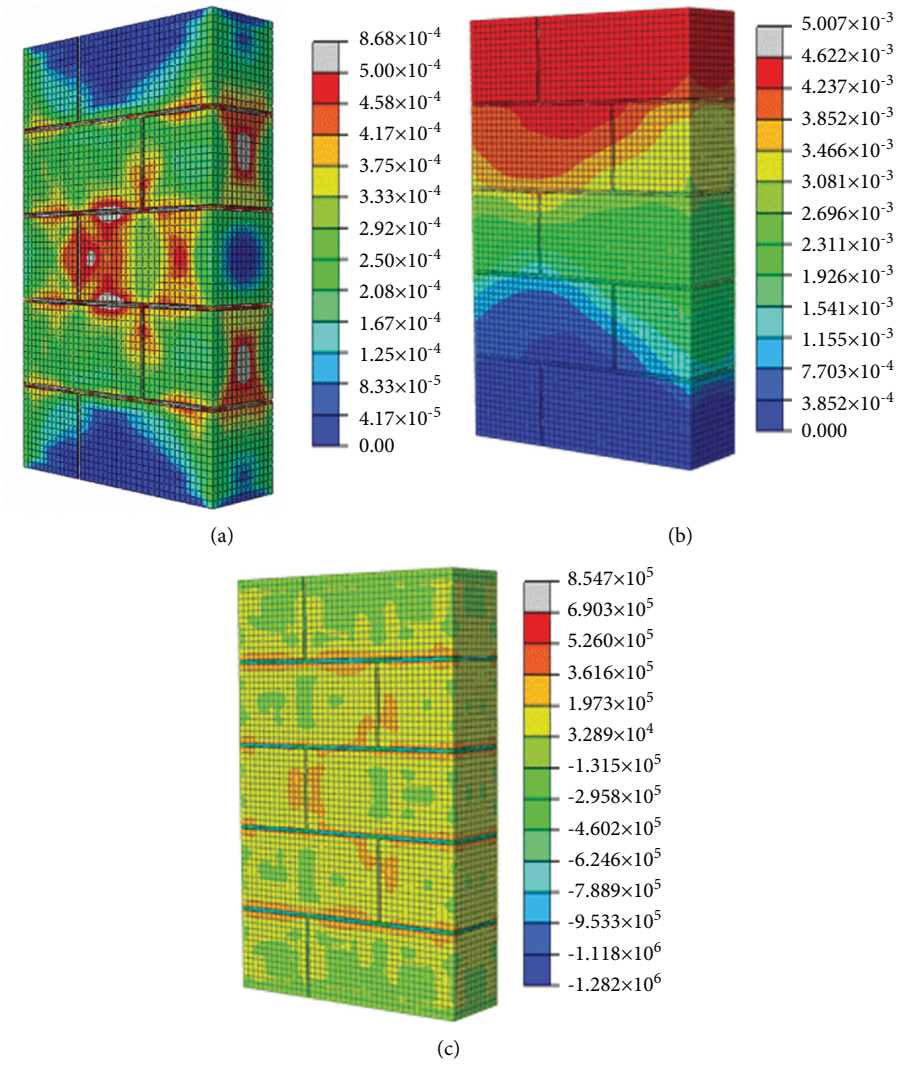

Figure 7: Simulation results. Cloud chart of (a) principle tensile strain, (b) displacement magnitude, and (c) 1st principle stress.

strain criterion. That is to say, the distribution of the principal tensile strain could reflect its failure pattern. Thus, according to the principle tensile strain cloud chart shown in Figure 7(a), cracks might be easy to form and distribute on the center part, the ITZ as well as the mortar, and the top as well as the bottom part. Compared with the failure mode shown in Figure 8, the simulation results were demonstrated to be similar to the test. The obvious cracks and damage could be observed in the masonry sample's center of the front face, the upper corner, and the center of the side face. These damaged parts matched the high-value area in the cloud chart of principle tensile strain. Meanwhile, these experimental and simulation results met the results and discussion reported in our previous studies [34, 35]. Thus, it could be noted that this simulation method would be suitable for analyses of concrete block masonry.

4.3. Effect of Concrete Block and Mortar Types. Based on the extended simulation analysis, the effect of component material properties on the masonry's compressive strengths would be discussed in this part. The relationship between the strength of masonry and components, i.e., the mortar and concrete block, is drawn in Figure 9.

The effect of mortar and concrete block strength on masonry compressive strength could then be observed: the increase of these two components' strength would cause the masonry's compressive strength to increase. Besides, the curves plotted in Figure 9 represented an obvious nonlinear relationship between the masonry compressive strength and the mortar. This simulation study produced results that corroborate the findings of a great deal of the previous work reported [17, 36].

Besides, the core procedure in this simulation method introduced was solving algebraic equations. Many efficient

(a) (b)

Figure 8: Experimental failure pattern. (a) Front view. (b) Side view.

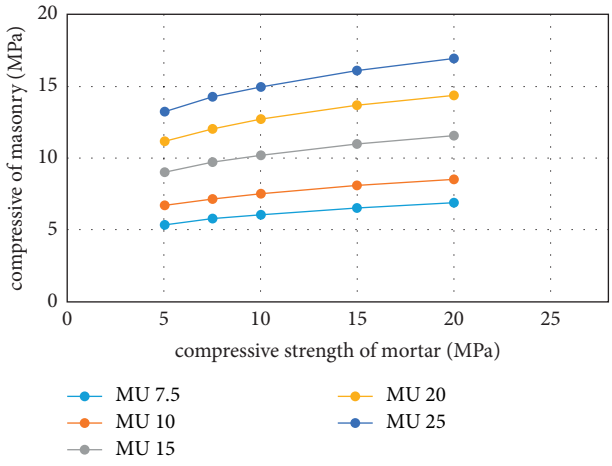

Figure 9: Effect of mortar and concrete block strength on masonry compressive strength.

and widely used methods for solving this sort of equation have been developed. Compared with other nonlinear solving methods based on iteration, the manner proposed in this study costs less computational resources.

5. Conclusions

This paper presented an alternative mesoscale approach for modeling concrete block masonry in which a simplistic representation of the mesomodel geometrical model consisting of the concrete block, the mortar, and the ITZ was provided. Additionally, the kill-FEM was successfully employed to solve the numerical model. The kill-FEM contributed significantly to reducing the computational cost since only a group of linear equations needs to be solved with a modified element stiffness matrix. According to the benchmark tests, the following conclusions arose:

(1) The mesoscale numerical method proposed was able to predict the main aspect of the failure behavior of concrete block masonry, i.e., the compressive strength as well as the failure pattern of the masonry.

(2) As a quasibrittle material, the concrete block masonry could be recognized as that meeting the

maximum tensile strain criterion. According to the principle tensile strain's cloud chart, cracks might be easy to form and distribute on the center part, the ITZ as well as the mortar, and the top as well as the bottom part.

(3) The positive effect of mortar and concrete block strength on masonry compressive strength was obtained according to the simulation studies. Besides, an obvious nonlinear relationship between the masonry compressive strength and the mortar was also observed.

The numerical method introduced in this paper provided a powerful tool for predicting and studying the concrete block masonry's observed macroscopic behavior. This study contributes to the characterization of the concrete block masonry mesostructure and the understanding of its influence on the macrobehavior. Furthermore, a proper understanding of the relationship between mesostructure and macroscopic behavior can guide the study of other systems containing advanced concrete production.

Data Availability

No data were used to support this study.

Conflicts of Interest

The authors declare that they have no conflicts of interest.

Acknowledgments

This work was supported by the Scientific Research Fund of Institute of Engineering Mechanics and the National Natural Science Foundation of China (Grant no. 52008135).

References

[1] G. Mohamad, P. B. Lourenço, and H. R. Roman, "Mechanics of hollow concrete block masonry prisms under compression: review and prospects," *Cement and Concrete Composites*, vol. 29, no. 3, pp. 181–192, 2007.

[2] A. Al-Fakih, M. M. A. Wahab, B. S. Mohammed, M. S. Liew, N. A. Wan Abdullah Zawawi, and S. As'ad, "Experimental study on axial compressive behavior of rubberized interlocking masonry walls," *Journal of Building Engineering*, vol. 29, Article ID 101107, 2020.

[3] K. Sajanthan, B. Balagasan, and N. Sathiparan, "Prediction of compressive strength of stabilized earth block masonry," *Advances in Civil Engineering*, vol. 2019, Article ID 2072430, 13 pages, 2019.

[4] A. Furtado, M. T. De Risi, H. Chaulagain, I. Misir, and T. Šipoš, "Recent advances on analysis methods and modelling approaches for seismic assessment and design of infilled rc buildings," *Advances in Civil Engineering*, vol. 2020, Article ID 4101826, 1 page, 2020.

[5] T. Zahra, M. Asad, and J. Thamboo, "Effect of geometry on the compression characteristics of bonded brickwork," *Structures*, vol. 32, pp. 1408–1419, 2021.

[6] M. Wang, X. Yang, and W. Wang, "Establishing a 3d aggregates database from x-ray ct scans of bulk concrete," *Construction and Building Materials*, vol. 315, Article ID 125740, 2022.

[7] Z. Ruijing and D. Hongzhe, "Independent component analysis-based arbitrary polynomial chaos method for stochastic analysis of structures under limited observations," *Mechanical Systems & Signal Processing*, vol. 173, Article ID 109026, 2020.

[8] D. Hongzhe, Z. Ruijing, and B. Miachel, "A new perspective on the simulation of cross-correlated random fields," *Structural Safety*, vol. 96, Article ID 102201, 2020.

[9] Z. Ruijing and D. Hongzhe, "A non-Gaussian stochastic model from limited observations using polynomial chaos and fractional moments," *Reliability Engineering and System Safety*, vol. 221, Article ID 108323, 2022.

[10] T. Zahra, A. Jelvehpour, J. A. Thamboo, and M. Dhanasekar, "Interfacial transition zone modelling for characterisation of masonry under biaxial stresses," *Construction and Building Materials*, vol. 249, Article ID 118735, 2020.

[11] P. G. Asteris, P. B. Lourenço, M. Hajihassani et al., "Soft computing-based models for the prediction of masonry compressive strength," *Engineering Structures*, vol. 248, Article ID 113276, 2021.

[12] A. Abasi, R. Hassanli, T. Vincent, and A. Manalo, "Influence of prism geometry on the compressive strength of concrete masonry," *Construction and Building Materials*, vol. 264, Article ID 120182, 2020.

[13] A. A. Hamid and A. O. Chukwunenye, "Compression behavior of concrete masonry prisms," *Journal of Structural Engineering*, vol. 112, no. 3, pp. 605–613, 1986.

[14] R. Sousa, J. Guedes, and H. Sousa, "Characterization of the uniaxial compression behaviour of unreinforced masonry-Sensitivity analysis based on a numerical and experimental approach," *Archives of Civil and Mechanical Engineering*, vol. 15, no. 2, pp. 532–547, 2015.

[15] M. M. Maras and M. M. Kose, "Structural behavior of masonry panels strengthened using geopolymer composites in compression tests," *Iranian Journal of Science and Technology, Transactions of Civil Engineering*, vol. 45, no. 2, pp. 767–777, 2021.

[16] E. Moradabadi, D. F. Laefer, J. A. Clarke, and P. B. Lourenço, "A semi-random field finite element method to predict the maximum eccentric compressive load for masonry prisms," *Construction and Building Materials*, vol. 77, pp. 489–500, 2015.

[17] C. S. Barbosa, P. B. Lourenço, and J. B. Hanai, "On the compressive strength prediction for concrete masonry prisms," *Materials and Structures*, vol. 43, no. 3, pp. 331–344, 2010.

[18] X. Wang, C. C. Lam, and V. P. Iu, "Characterization of mechanical behaviour of grey clay brick masonry in China," *Construction and Building Materials*, vol. 262, Article ID 119964, 2020.

[19] G. Milani, "Simple homogenization model for the non-linear analysis of in-plane loaded masonry walls," *Computers & Structures*, vol. 89, no. 17-18, pp. 1586–1601, 2011.

[20] C. A. Filippou, N. C. Kyriakides, and C. Z. Chrysostomou, "Numerical modelling and simulation of the in-plane response of a three-storey masonry-infilled rc frame retrofitted with trm," *Advances in Civil Engineering*, vol. 2020, Article ID 6279049, 19 pages, 2020.

[21] F. Zhu, Q. Zhou, F. Wang, and X. Yang, "Spatial variability and sensitivity analysis on the compressive strength of hollow concrete block masonry wallettes," *Construction and Building Materials*, vol. 140, pp. 129–138, 2017.

[22] J. Álvarez-Pérez, J. H. Chávez-Gómez, B. T. Terán-Torres, M. Mesa-Lavista, and R. Balandrano-Vázquez, "Multifactorial behavior of the elastic modulus and compressive strength in masonry prisms of hollow concrete blocks," *Construction and Building Materials*, vol. 241, Article ID 118002, 2020.

[23] E. Nasiri and Y. Liu, "Development of a detailed 3d fe model for analysis of the in-plane behaviour of masonry infilled concrete frames," *Engineering Structures*, vol. 143, pp. 603–616, 2017.

[24] J. A. Thamboo and M. Dhanasekar, "Nonlinear finite element modelling of high bond thin-layer mortared concrete masonry," *International Journal of Magnetic Resonance Imaging*, vol. 1, no. 1, pp. 5–26, 2016.

[25] T. Zahra, J. Thamboo, and M. Asad, "Compressive strength and deformation characteristics of concrete block masonry made with different mortars, blocks and mortar beddings types," *Journal of Building Engineering*, vol. 38, Article ID 102213, 2021.

[26] M. Bolhassani, A. A. Hamid, A. C. W. Lau, and F. Moon, "Simplified micro modeling of partially grouted masonry assemblages," *Construction and Building Materials*, vol. 83, pp. 159–173, 2015.

[27] M. Angiolilli, M. Pathirage, A. Gregori, and G. Cusatis, "Lattice discrete particle model for the simulation of irregular stone masonry," *Journal of Structural Engineering*, vol. 147, no. 9, Article ID 04021123, 2021.

[28] G. Giambanco and Z. Mróz, "The interphase model for the analysis of joints in rock masses and masonry structures," *Meccanica*, vol. 36, no. 1, pp. 111–130, 2001.

[29] S. Nazir and M. Dhanasekar, "Modelling the failure of thin layered mortar joints in masonry," *Engineering Structures*, vol. 49, pp. 615–627, 2013.

[30] S. Nazir and M. Dhanasekar, "A non-linear interface element model for thin layer high adhesive mortared masonry," *Computers & Structures*, vol. 144, pp. 23–39, 2014.

[31] A. Caballero, C. M. López, and I. Carol, "3d meso-structural analysis of concrete specimens under uniaxial tension," *Computer Methods in Applied Mechanics and Engineering*, vol. 195, no. 52, pp. 7182–7195, 2006.

[32] N. Schlömer, "meshio: tools for mesh files," https://github.com/nschloe/meshio.

[33] K. M. Lee and J. H. Park, "A numerical model for elastic modulus of concrete considering interfacial transition zone," *Cement and Concrete Research*, vol. 38, no. 3, pp. 396–402, 2008.

[34] Q. Zhou, F. Wang, F. Zhu, and X. Yang, "Stress-strain model for hollow concrete block masonry under uniaxial compression," *Materials and Structures*, vol. 50, no. 2, p. 106, 2017.

[35] X. Yang, F. Wang, X. Yang, and Q. Zhou, "Fractal dimension in concrete and implementation for meso-simulation," *Construction and Building Materials*, vol. 143, pp. 464–472, 2017.

[36] V. G. Haach, G. Vasconcelos, and P. B. Lourenço, "Assessment of compressive behavior of concrete masonry prisms partially filled by general mortar," *Journal of Materials in Civil Engineering*, vol. 26, no. 10, Article ID 04014068, 2014.